Rare Met. (2021) 40(8):2033–2039
https://doi.org/10.1007/s12598-020-01473-7

RARE METALS
www.editorialmanager.com/rmet

ORIGINAL ARTICLE

Preparation and properties of hot-deformed magnets processed from nanocrystalline/amorphous Nd–Fe–B powders

Peng Zhao, Yang Luo*, Dun-Bo Yu, Hai-Jun Peng, Wen-Long Yan, Zi-Long Wang, Xin-Yuan Bai

Received: 4 March 2019 / Revised: 9 May 2019 / Accepted: 25 May 2020 / Published online: 17 July 2020

Abstract The hot-deformed magnets processed from nanocrystalline/amorphous Nd–Fe–B powders were prepared under different hot-pressing temperatures (600–750 °C, at intervals of 25 °C) by the self-made hot-pressing equipment. The microstructure and magnetic properties of hot-deformed magnets prepared at different temperatures were also investigated. When the temperature is above 650 °C, the density of magnet reaches 7.5 g·cm^{-3}. The optimum magnetic properties of magnetic induction intensity of B_r = 1.3 T, optimum energy product of $(BH)_{max}$ = 282.5 kJ·m^{-3}, intrinsic coercivity of H_{cj} = 1130.0 kA·m^{-1} of hot-deformed magnets are obtained at hot-pressing temperature of 650 °C. X-ray diffractometer pattern shows that the (00L) texture has been obtained. For the microstructural characteristic, on the one hand, the good magnetic performance is attributed to the fine platelet-like grains with an average length of 410–440 nm at the hot-pressing temperature range from 625 to 675 °C. On the other hand, the unaligned coarse grains are observed in all the samples. And the areal fraction of those is gradually increasing with the rise of the hot-pressing temperature, which tends to deteriorate the magnetic properties. The composition map shows the accumulation of Nd/Pr-rich phase in the coarse grains' region.

P. Zhao, Y. Luo*, D.-B. Yu, H.-J. Peng, W.-L. Yan, Z.-L. Wang, X.-Y. Bai
National Engineering Research Center for Rare Earth Materials, General Research Institute for Nonferrous Metals, Beijing 100088, China
e-mail: eluoyang@foxmail.com

Y. Luo, D.-B. Yu, H.-J. Peng, W.-L. Yan, Z.-L. Wang, X.-Y. Bai
Grirem Advanced Materials Co., Ltd, Beijing 100088, China

Keywords Nanocrystalline/amorphous powders; Hot-pressing temperature; Hot-deformed Magnets; Magnetic properties; Microstructure

1 Introduction

Excellent magnetic properties of permanent magnets depend on the high coercivity and the high remanence, with a good squareness (Q) of the demagnetization curves [1–8]. Thus, hot-deformed technique draws much attention in recent years, since it can generate a good grain alignment (good texture) and nanocrystalline microstructure [9]. Generally, the hot-deformed process can be applied to melt-spun [10–13] or hydrogenation disproportionation desorption recombination (HDDR) [14, 15] Nd–Fe–B materials. The hot-deformed magnets are obtained by hot-pressing (HP) process and hot-deforming (HD) process. The initial powders can be fully compacted by hot-pressing process, and then, the hot-pressed magnets are further deformed to obtain the hot-deformed magnets [16–20]. Compared with the sintered Nd–Fe–B magnets, the hot-deformed Nd–Fe–B magnets have low content of rare-earth, good thermal stability and corrosion resistance. Hot-deformed Nd–Fe–B magnets have been prepared by Lee et al. [21] in 2003 and exhibit good magnetic properties.

A great number of researches are devoted to improving the properties of hot-deformed magnets. Recently, a new method of coercivity enhancement has been discovered by Hono et al. [22]. The result demonstrates that hot-deformed magnets processed from amorphous powders show higher coercivity than that processed from nanocrystalline powder. And that is different from the method of grain boundary modification [23, 24]. Because of the high

temperature, the grains will grow and the magnetic properties are very sensitive to the grain size [25]. The dependence of magnetic properties on hot-deformed temperature has been concerned.

For nanocrystalline magnetic powers, numerous researches about hot-pressing temperature and hot-deformed temperature have been conducted. The density and the grain size of hot-pressed magnets are affected by the hot-pressing temperature, which further affects the microstructure and the properties of hot-deformed magnets. The effect of hot-pressing temperature ranges from 550 to 780 °C on density and magnetic properties of hot-deformed magnets has been discussed by Lipiec and Davies [16]. The hot-deformed temperature is another important temperature parameter, and it greatly affects the ability of deformation [26], microstructure [27], density [28], magnetic and mechanical [29] properties.

All the above studies focus on the hot-deformed magnets with nanocrystalline precursor. Nevertheless, few reports have systematically studied the effect of temperature on the microstructures and magnetic performance of the hot-deformed magnets processed from nanocrystalline/amorphous melt-spun Nd–Fe–B powders. This work aims to prepare the hot-deformed magnets processed from nanocrystalline/amorphous melt-spun Nd–Fe–B powders and investigate the effect of hot-pressing temperature on phase structure, microstructure and magnetic properties for the hot-pressed and hot-deformed magnets, respectively. Finally, the optimum hot-pressing temperature range is obtained, at which hot-deformed magnet with good magnetic performance is prepared.

2 Experimental

The alloy ingots with a nominal composition of $(Pr,Nd)_{28.87}Fe_{bal}.Co_{3.35}Ga_{0.49}B_{0.91}$ (wt%) were prepared by induction melting. And then, the melt-spun ribbons were obtained by single-roller melt-quenching at a wheel speed of 40 $m{\cdot}s^{-1}$ under Ar atmosphere, pulverized to initial magnetic powders with particle size of 120–180 μm. Subsequently, with the self-made hot-pressing equipment, the dense cylindrical magnets were prepared by hot-pressing at 600–750 °C under 100 MPa in vacuum, and then, these cylindrical magnets were further hot-deformed to obtain wafer magnets at 725 °C at an average of 0.03 $mm{\cdot}s^{-1}$ until 70% reduction in height was achieved. The small cylinders with 2.5 mm in diameter were cut from the middle of the wafer magnets by an electric spark linear cutting. The overall structure of the samples was identified by X-ray diffractometer (XRD, Rigaku, Smartlab) with Co Kα radiation. The magnetic properties were measured by vibrating sample magnetometer (VSM, Quantum Design, Versalab). The microstructure of the samples was obtained by scanning electron microscope (SEM, ZEISS). Energy-dispersive spectrometry (EDS) was used to investigate the mapping of composition.

3 Results and discussion

3.1 Initial magnetic powder

Figure 1 shows the hysteresis loop and diffraction pattern of initial powder. In Fig. 1a, a kink can be observed in the second quadrant of the hysteresis loop, meaning the existence of amorphous phase or other phases. In Fig. 1b, XRD result demonstrates that the sample consists of $Nd_2Fe_{14}B$ phase, and no other phases were detected compared with the standard PDF-card. It has been reported that the amorphous phase is obtained easily because of the rapid quench at higher wheel speed [30]. So, the nanocrystalline/amorphous Nd–Fe–B powders have been already prepared.

3.2 Hot-pressed magnets

The density and magnetic properties of hot-pressed magnets under different hot-pressing temperatures are shown in Fig. 2. It can be seen that the density of hot-pressed magnets increases as the hot-pressing temperature goes up. The density rises from 7.0 to 7.3 g cm^{-3} when the hot-pressing temperature goes from 600 to 625 °C. When the hot-pressing temperature is above 650 °C, the density reaches 7.5 $g{\cdot}cm^{-3}$. The remanence gradually rises with the hot-pressing temperature increasing from 600 to 650 °C and then enters in a plateau with the temperature further rising, which is consistent with the relationship between temperature and the density. Meanwhile, the coercivity is gradually decreasing as the temperature is above 675 °C. On the one hand, the high hot-pressing temperature leads to the higher density and the lower content of the non-magnetic phase, which is beneficial to the properties of the magnets [16]. On the other hand, the high hot-pressing temperature will result in the increase in grain size in the magnets, which is bad for the performance. Therefore, strictly controlling the hot-pressing temperature is significant to obtain the hot-pressed magnets with high performance.

Figure 3 shows the fracture morphology of hot-pressed magnets. As shown in Fig. 3, the grains of hot-pressed magnet under 650 °C are finer than those under 750 °C. The lower coercivity of magnets at 750 °C is attributed to the abnormal grain growth [28]. Thus, the hot-pressed magnets with optimum magnetic properties and fine grains can be obtained at 650–675 °C.

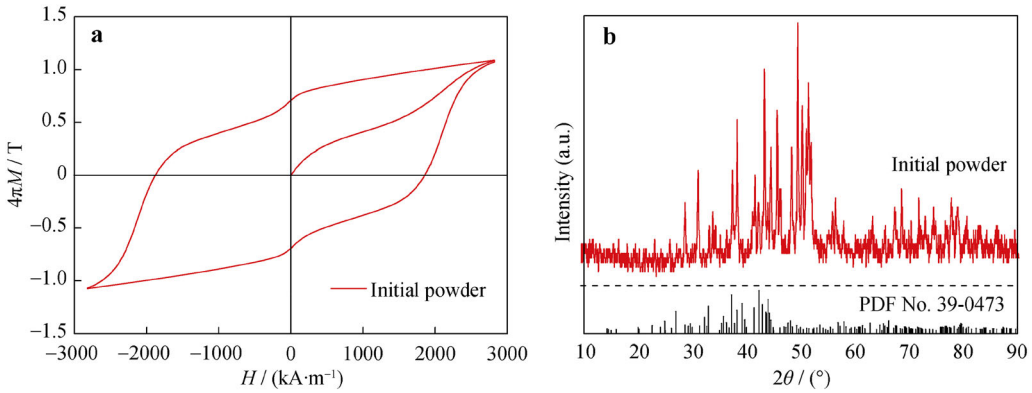

Fig. 1 **a** Hysteresis loop and **b** XRD pattern of initial powder

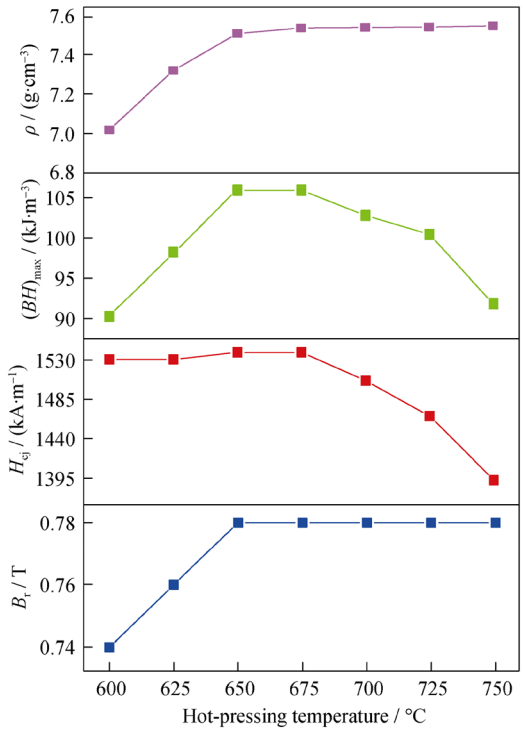

Fig. 2 Magnetic properties and density of hot-pressed magnets dependence of hot-pressing temperature

3.3 Hot-deformed magnets

Figure 4 shows the dependence of magnetic performance of hot-deformed magnets on hot-pressing temperature. The magnetic properties of hot-deformed magnets firstly improve and then deteriorate with the increase in the hot-pressing temperature. The optimum coercivity is obtained when the temperature reaches 625 °C, and then, the coercivity slowly declines between 625 and 675 °C. Dramatical reduction in coercivity happens when the temperature is higher. The optimum energy product ($(BH)_{max}$) and the remanence are obtained at 650 °C. The optimum Q value is obtained at 675 °C. The optimum comprehensive magnetic properties of magnetic induction intensity of B_r = 1.3 T, intrinsic coercivity of H_{cj} = 1130.0 kA·m^{-1}, $(BH)_{max}$ = 282.5 kJ·m^{-3}, Q = 0.57 are obtained.

Figure 5a shows the initial magnetization curves and demagnetization curves of hot-deformed magnets prepared at different hot-pressing temperatures. The shape of the initial magnetization curve shows a two-step behavior and changes as the hot-pressing temperature increases. As shown in Fig. 5a, b, a kink can be found in the second quadrant of the demagnetization curve and changes gradually with the increase in the hot-pressing temperature.

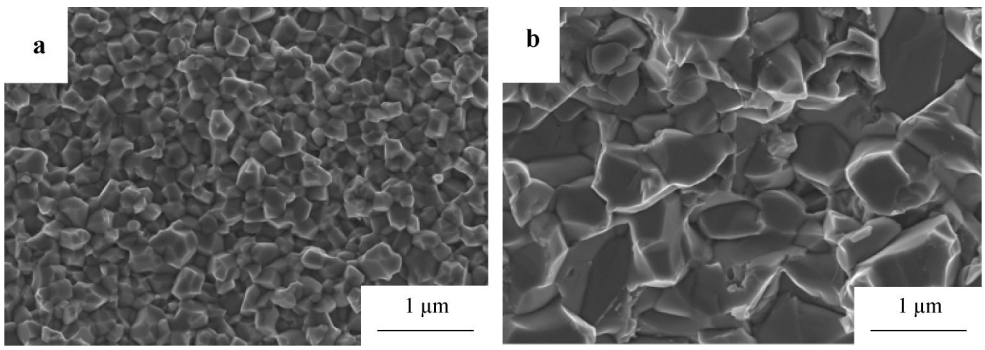

Fig. 3 Fracture SEM images of hot-pressed magnets at **a** 650 °C and **b** 750 °C

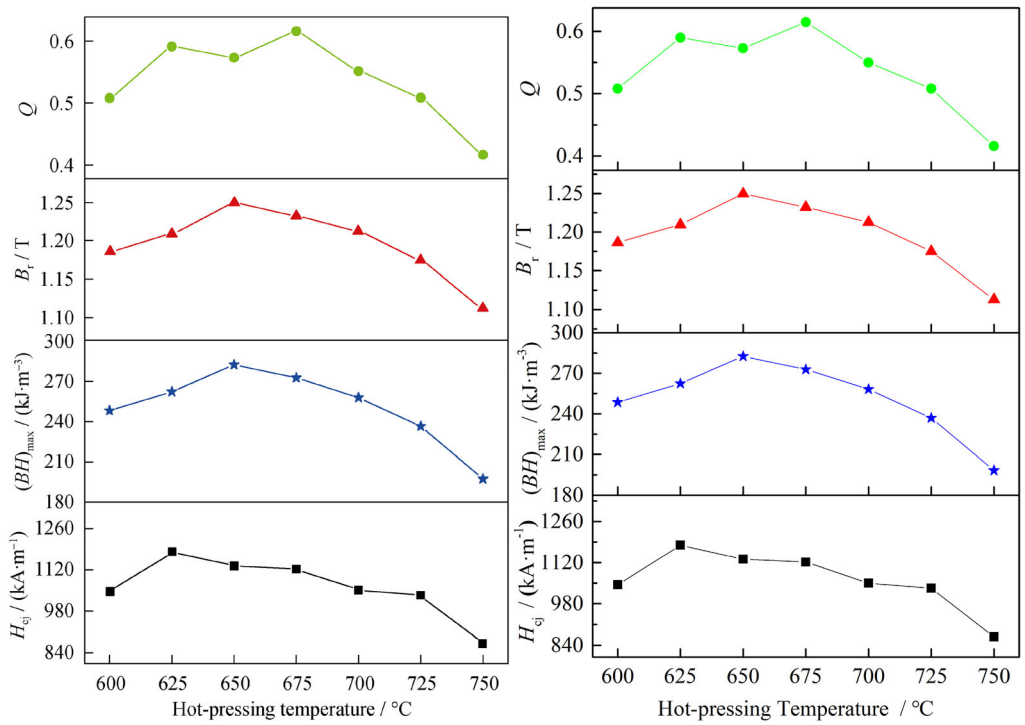

Fig. 4 Dependence of magnetic performance of hot-deformed magnets on different hot-pressing temperatures

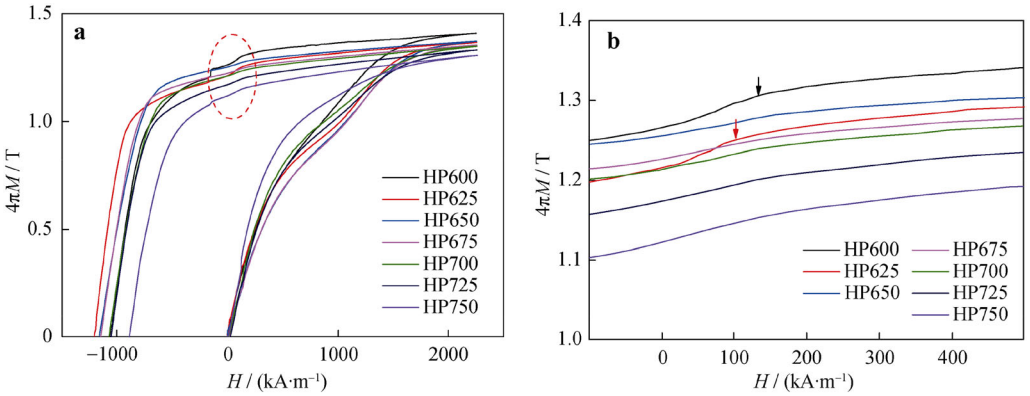

Fig. 5 **a** Initial magnetization curves and demagnetization curves of hot-deformed magnets at different hot-pressing temperatures; **b** magnified image of red circle (HP600-HP750 referred to the magnet hot-pressed at 600-750 °C)

When the hot-pressing temperature is in the range of 650–700 °C, the demagnetization curves become smooth. According to Refs. [25, 31–33], all the demagnetization curves are smooth. And XRD results in Fig. 6 demonstrate that there are no other phases. One possible reason for the appearance of the kink in the demagnetization curves is the existence of the amorphous phase in the samples.

In order to explore the difference of magnetic properties, magnetization behaviors and demagnetization behaviors, the phase structure and microstructure characteristics of hot-deformed magnets were investigated. XRD patterns and ratio of (105) peaks to (006) peaks of hot-deformed magnets at different hot-pressing temperatures are shown in Fig. 6. XRD patterns show that the samples consist of $Nd_2Fe_{14}B$ phase, and no other phases are detected. The major peaks of XRD are Peak (105) and Peak (00*L*), showing better crystallographic alignment [34–36]. As shown in Fig. 6a, the (00*l*) peaks of hot-deformed Nd–Fe–B magnets with better alignment gradually change with the hot-pressing temperature increasing. In order to understand the *c*-axis alignment, Fig. 6b shows that the ratio of (006) peaks to (105) peaks firstly increases and then drops with the hot-pressing temperature increasing. The variance of ratio keeps pace with that of the remanence in Fig. 4. When the temperature is higher than 650 °C, the ability of grain orientation is weakened due to the excessive hot-pressing

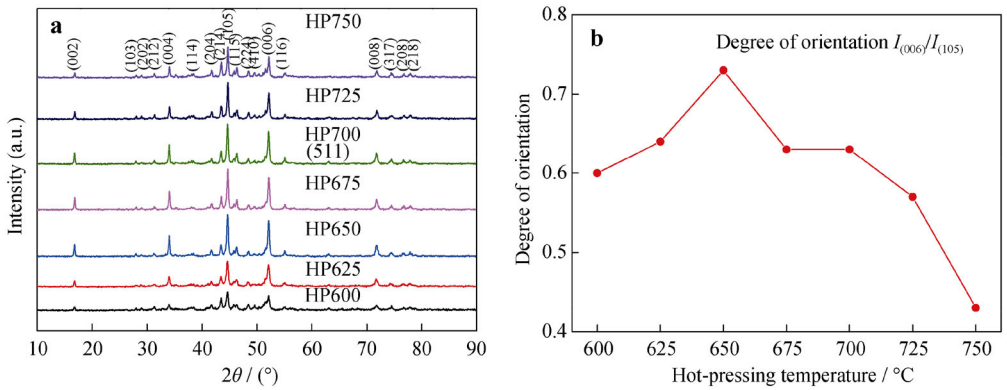

Fig. 6 **a** XRD patterns and **b** ratio of (105) peaks to (006) peaks of hot-deformed magnets at different hot-pressing temperatures

temperature. When the hot-pressing temperature is conducted at 750 °C, the deteriorating orientation in Fig. 6 can be ascribed to the abnormal grain growth shown in Fig. 3.

In order to figure out the influence of the microstructure on the magnetic properties, the fracture morphology of the hot-deformed magnets at hot-pressing temperature of 600–750 °C is characterized. Figure 7 shows the microstructure (× 20,000) of hot-deformed magnets with different hot-pressing temperatures. As shown in Fig. 7, the platelet-like grains can be found in all samples, and the existence of such platelet-like grains indicates that the *c*-axis orientation can be obtained by the hot-deformed process, but oriented degree of each sample is different.

Figure 8 shows the statistical grain size of hot-deformed magnets prepared at different hot-pressing temperatures. The length of the platelet-like grains of hot-deformed magnets varies with the elevated hot-pressing temperature. When the hot-pressing temperature is about 600 °C, the average length of the platelet-like grains is 250 nm, and then 410–440 nm at 625–675 °C, corresponding to the samples with good magnetic properties. As the hot-pressing temperature is higher than 700 °C, the average length of the platelet-like grains is above 500 nm. The abnormal grain growth leads to the decrease in coercivity of magnets [25, 28]. But for all samples, the width of the platelet-like grains is about (100 ± 10) nm, and the change of width is not obvious with enhanced hot-pressing temperature.

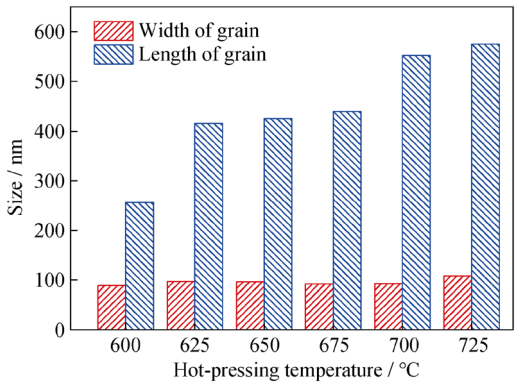

Fig. 8 Statistical grain size of hot-deformed magnets prepared at different hot-pressing temperatures

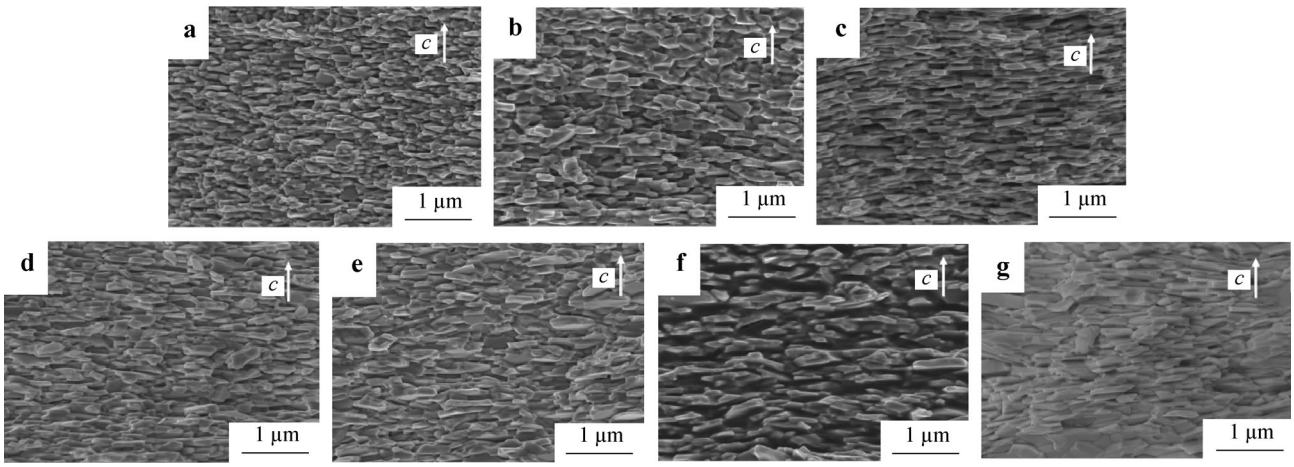

Fig. 7 Fracture SEM images of hot-deformed magnets prepared at different hot-pressing temperatures: **a** 600 °C, **b** 625 °C, **c** 650 °C, **d** 675 °C, **e** 700 °C, **f** 725 °C and **g** 750 °C

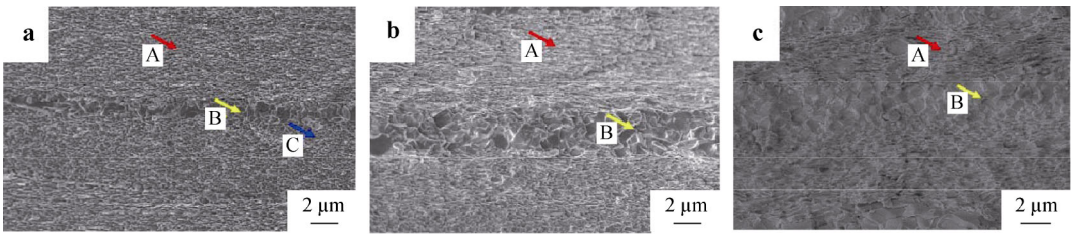

Fig. 9 Fracture SEM images of hot-deformed magnets prepared at different hot-pressing temperatures: **a** 600 °C, **b** 675 °C and **c** 750 °C

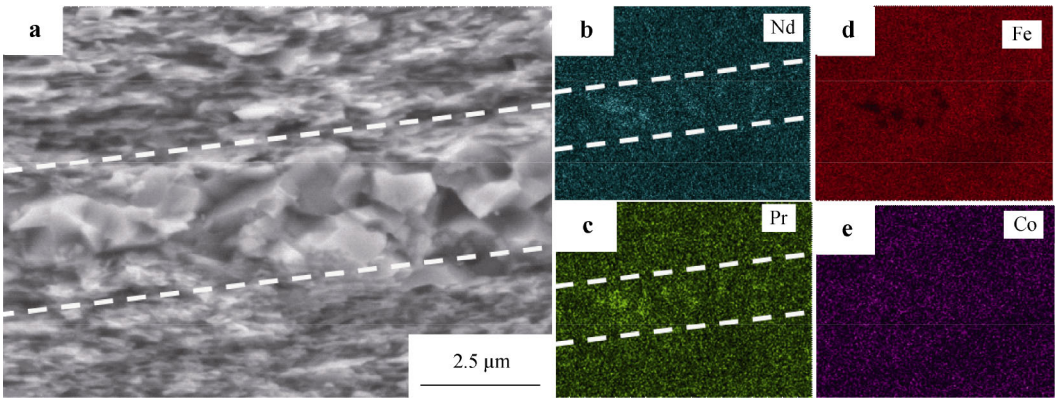

Fig. 10 **a** SEM image of hot-deformed magnets prepared at hot-pressing temperature of 675 °C; EDS mapping of same region for **b** Nd, **c** Pr, **d** Fe and **e** Co

As shown in Fig. 9, the layers in the microstructure (× 5000) were characterized, and the zone of unaligned large grains gradually enlarges with the increase in the hot-pressing temperature. At 600 °C, three states of grains platelet-like grains, unaligned fine equiaxed grains and unaligned coarse equiaxed grains exist in the magnets, as shown by the arrows in Fig. 9. The unaligned fine equiaxed grains disappear at 675 °C, and the platelet-like grains and unaligned coarse equiaxed grains account for the main part. Abnormal grain growth happens at 750 °C; meanwhile, the unaligned coarse grains occupy most of the volume in the magnets. The large grains are unaligned, so the existence of large grains accounts for the worsening magnetic properties.

The microstructure and mapping of hot-deformed magnets hot-pressed at 675 °C are shown in Fig. 10. In the coarse grains' region, there is obvious accumulation of rare-earth elements such as Nd and Pr, and the rare-earth elements content in the coarse grains' region is obviously higher than that in the fine grains' region. The liquid grain boundary phase will be extruded into the interspaces in ribbon interfaces with great stress at high temperature, which is the main reason of grain growth. There are many defects between layers, and disappearance of the interface will release energy, which will promote the nucleation of grain [26].

4 Conclusion

In this study, the influence of hot-pressing temperature on microstructural evolution and the magnetic performance of hot-deformed magnets processed from nanocrystalline/amorphous melt-spun Nd–Fe–B alloys were systematically investigated. It is found that the density of hot-pressed magnets reaches 7.5 g·cm^{-3} as the temperature is above 650 °C. The optimum magnetic performance of B_r = 1.3 T, $(BH)_{max}$ = 282.5 kJ·m^{-3}, H_{cj} = 1130.0 kA·m^{-1} of hot-deformed magnets is obtained at hot-pressing temperature of 650 °C. When the hot-pressing temperature is at 625–675 °C, the platelet-like grains are fine with the average length of 410–440 nm, benefitting to obtain good magnetic properties. The unaligned coarse grains are observed at all the samples, and the zone of those is gradually increasing with the increase in the hot-pressing temperature. The layers tend to lower the magnetic properties. The EDS shows the accumulation of Nd/Pr-rich phase in the coarse grain's region.

Acknowledgements This work was financially supported by the National Key Research and Development Program (No. 2016YFB0700902).

References

[1] Volkov VV, Zhu Y. Magnetic structure and microstructure of die-upset hard magnets $RE_{13.75}Fe_{80.25}B_6$ (RE = Nd, Pr) A possible origin of high coercivity. J Appl Phys. 1999;85(6):3254.

[2] Ju J, Wang Z, Yan A. Near-surface microstructure improvement for die-upset Nd–Fe–B magnets with an enhanced maximum energy product. J Alloy Compd. 2017;710:66.

[3] Ma BM, Brown D, Chen ZM. Developments in the processing and properties of NdFeb-type permanent magnets. J Magn Magn Mater. 2002;248:432.

[4] Lei W, Yu Y, Yang W, Feng M, Li H. A general strategy for synthesizing high-coercivity L10-FePt nanoparticles. Nanoscale. 2017;9(35):12855.

[5] Lei W, Xu J, Yu Y, Yang W, Hou Y, Chen D. Halide ion-mediated synthesis of L10-FePt nanoparticles with tunable magnetic properties. Nano Lett. 2018;18(12):7839.

[6] Yang W, Yu Y, Wang L, Yang C, Li H. Controlled synthesis and assembly into anisotropic arrays of magnetic cobalt-substituted magnetite nanocubes. Nanoscale. 2015;7(7):2877.

[7] Yang W, Lei W, Yu Y, Zhu W, George TA, Li XZ, Sellmyer DJ, Sun S. From FePt–Fe_3O_4 to L10-FePt–Fe nanocomposite magnets with a gradient interface. J Mater Chem C. 2015;3(27):7075.

[8] Yu Y, Mukherjee P, Tian Y, Li XZ, Shield JE, Sellmyer DJ. Direct chemical synthesis of L10-FePtAu nanoparticles with high coercivity. Nanoscale. 2014;6(20):12050.

[9] Yasuda HY, Kumano M, Nagase T, Kato R, Shimizu H. Tensile deformation behavior of Nd–Fe–B alloys. Scr Mater. 2011;65(8):743.

[10] Li L, Graham CD. Mechanism of texture formation by hot deformation in rapidly quenched FeNdB. J Appl Phys. 1990;67(9):4756.

[11] Yi P, Lee D, Yan A. Effects of compositions on characteristics and microstructures for melt-spun ribbons and die-upset magnets of $Nd_{12.8+x}Fe_{81.2-x-y-z}Co_yGa_zB_6$. J Magn Magn Mater. 2010;322:3019.

[12] Wang YL, Luo Y, Wang ZL, Wu GY, Xie JJ, Yan WL, Yu DB. Coercivity enhancement in Nd–Fe–B magnetic powders by Nd–Cu–Al grain boundary diffusion. J Magn Magn Mater. 2018;458:85.

[13] Tian H, Jin DZ, Li Y, Zhu MY, Jin HM. Microstructure and magnetic properties of anisotropic Nd–Fe–B magnets fabricated by single-stage hot deformation. J Rare Earths. 2006;24(1):318.

[14] Wang H, Chen R, Yin W, Zhu M, Tang X, Wang Z, Jin C, Ju J, Lee D, Yan A. The effect of Nd–Cu diffusion during hot pressing and hot deformation on the coercivity and the deformation ability of Nd–Fe–B HDDR magnets. J Magn Magn Mater. 2017;438:35.

[15] Kirchner A, Liesert S. Preparation of anisotropic NdFeB magnets with different Nd contents by hot deformation (die-upsetting) using hot-pressed HDDR powders. J Alloy Compd. 1998;266:260.

[16] Lipiec W, Davies HA. The influence of the powder densification temperature on the microstructure and magnetic properties of anisotropic NdFeB magnets aligned by hot deformation. J Alloy Compd. 2010;491(1–2):694.

[17] Liu J, Sepehri-Amin H, Ohkubo T, Hioki K, Hattori A, Schrefl T, Hono K. Effect of Nd content on the microstructure and coercivity of hot-deformed Nd–Fe–B permanent magnets. Acta Mater. 2013;61(14):5387.

[18] Hou YH, Wang YL, Huang YL, Wang Y, Li S, Ma SC, Liu ZW, Zeng DC, Zhao LZ, Zhong ZC. Effects of Nd-rich phase on the improved properties and recoil loops for hot deformed Nd–Fe–B magnets. Acta Mater. 2016;115:385.

[19] Zhang T, Chen F, Zheng Y, Wen H, Wang J, Zhang L, Zhou L. Hot-deformed Nd–Fe–B magnets fabricated by dynamic loading with a high maximum energy product. Intermetallics. 2016;73:67.

[20] Wang XC, Zhu MG, Li W, Li YF, Lai B, Du A. Microstructure and magnetic properties of anisotropic hot-deformed magnet of different magnetic particle sizes. Rare Met. 2015;34(4):255.

[21] Lee D, Hilton JS, Liu S, Zhang Y, Hadjipanayis GC, Chen CH. Hot-pressed and hot-deformed nanocomposite (Nd, Pr, DY)2Fe14B/alpha-Fe-based magnets. IEEE Trans Magn. 2003;39(5):2947.

[22] Tang X, Sepehri-Amin H, Ohkubo T, Hioki K, Hattori A, Hono K. Coercivities of hot-deformed magnets processed from amorphous and nanocrystalline precursors. Acta Mater. 2017;123:1.

[23] Liu WQ, Chang C, Yue M, Yang JS, Zhang DT, Zhang JX, Liu YQ. Coercivity, microstructure, and thermal stability of sintered Nd–Fe–B magnets by grain boundary diffusion with TbH3 nanoparticles. Rare Met. 2017;36(9):718.

[24] Wang JM, Guo ZH, Jing Z, Du X, Yu NJ, Li MY, Zhu MG, Li M. Coercivity enhancement of hot-deformed Nd–Fe–B magnets with Pr–Cu alloy addition. Rare Met. 2018. https://doi.org/10.1007/s12598-017-0993-7.

[25] Liu J, Sepehri-Amin H, Ohkubo T, Hioki K, Hattori A, Schrefl T, Hono K. Grain size dependence of coercivity of hot-deformed Nd–Fe–B anisotropic magnets. Acta Mater. 2015;82:336.

[26] Lai B, Liu GJ, Wang HJ, Pan W, Zhu MG. Effect of hot-deformed temperature on magnetic properties of nanograin Nd–Fe–B magnets. Met Funct Mater. 2011;3:1.

[27] Kwon H. Effect of grain size and die-upset temperature on texture in die-upset Nd–Fe–B magnet. IEEE Trans Magn. 2009;45:2590.

[28] Lin M, Wang HJ, Yi PP, Yan AR. Effects of excessive grain growth on the magnetic and mechanical properties of hot-deformed NdFeB magnets. J Magn Magn Mater. 2010;322(15):2268.

[29] Hu ZH, Li J, Chu LH, Liu Y. Effect of hot deformation temperature on the magnetic and mechanical properties of Nd–Fe–B magnets prepared by spark plasma sintering. J Magn Magn Mater. 2011;323(1):104.

[30] Li Z, Zhang M, Shen BG, Hu FX, Sun JR. Permanent magnetic properties of rapidly quenched $(La, Ce)_2Fe_{14}B$ nanomaterials based on La–Ce mischmetal. J Alloy Compd. 2015;651:144.

[31] Skoug EJ, Meyer MS, Pinkerton FE, Tessema MM, Haddad D, Herbst JF. Crystal structure and magnetic properties of $Ce_2Fe_{14-x}Co_xB$ alloys. J Alloy Compd. 2013;574:552.

[32] Liu L, Sepehri-Amin H, Ohkubo T, Yano M, Kato A, Sakuma N, Shoji T, Hono K. Coercivity enhancement of hot-deformed Nd–Fe–B magnets by the eutectic grain boundary diffusion process using $Nd_{62}Dy_{20}Al_{18}$ alloy. Scr Mater. 2017;129:44.

[33] Tang X, Chen R, Li M, Jin C, Yin W, Lee D, Yan A. Grain boundary diffusion behaviors in hot-deformed $Nd_2Fe_{14}B$ magnets by PrNd-Cu low eutectic alloys. J Magn Magn Mater. 2018;445:66.

[34] Liu Y, Xu L, Wang Q, Li W, Zhang X. Development of crystal texture in Nd-lean amorphous $Nd_9Fe_{85}B_6$ under hot deformation. Appl Phys Lett. 2009;94(17):172502.

[35] Lee YI, Huang GY, Shih CW, Chang WC, Chang HW, You JS. Coercivity enhancement in hot deformed $Nd_2Fe_{14}B$ -type magnets by doping low-melting RCu alloys (R = Nd, Dy, Nd + Dy). J Magn Magn Mater. 2017;439:1.

[36] Li M, Chen R, Jin C, Yu J, Tang X, Chen G, Sun J, Wang Z, Yan A. Texture and microstructure improvement of hot-deformed magnets with platelet-like nano h-BN addition. Scr Mater. 2018;152:127.